THE ASTROPHYSICAL JOURNAL, 418:235–243, 1993 November 20

VLA RADIO RECOMBINATION LINE OBSERVATIONS OF IONIZED GAS IN THE −30 KILOMETERS PER SECOND MOLECULAR CLOUD (G0.04+0.03) NEAR THE GALACTIC CENTER. I. THE DISCRETE RADIO SOURCES

JUN-HUI ZHAO,[1] K. DESAI,[1,2] W. M. GOSS,[1] AND F. YUSEF-ZADEH[3]
Received 1993 February 19; accepted 1993 May 25

ABSTRACT

Multifrequency spectral line and continuum observations of ionized gas in the -30 km s^{-1} molecular cloud (G0.04+0.03) have been carried out using the VLA to study the nature of the discrete radio sources located between Sgr A West ($l = 0°$) and the arched filaments of the continuum arc ($l = 0°.2$). Spectral indices determined from 6 and 20 cm continuum data indicate that the spectra of these sources are flat or rising with frequency. Radio morphologies and the detection of radio recombination lines (H110α and H92α) confirm that these sources are H II regions. The line emission arises at negative radial velocities (-60 to -20 km s^{-1}), forbidden at these longitudes in the sense of Galactic rotation. The kinematics of the ionized gas suggest a close relationship with the molecular cloud observed in CS and ^{13}CO at a mean radial velocity of -30 km s^{-1} (G0.04+0.03). We derive LTE electron temperatures in the range 3500–7200 K. The low inferred electron temperatures may indicate relatively high metal abundances in these regions. The thermal sources are spatially correlated with [C II] 158 μm emission peaks and with the distribution of warm dust as indicated by the color temperature, T_c(55/125 μm). Overall, their properties and environments indicate that these H II regions are ionized by UV radiation from recently formed early-type stars in the molecular cloud at -30 km s^{-1}.

Subject headings: Galaxy: center — H II regions — ISM: molecules — ISM: structure — radio continuum: interstellar

1. INTRODUCTION

There is growing evidence for star formation activity in the Galactic center. Several H II regions, e.g., the Sgr A East H II complex (Ekers et al. 1983; Goss et al. 1983) and the H II region G (5′ south of Sgr A West [Ho et al. 1985; Armstrong, Jackson, & Ho 1989]) have been studied with the Very Large Array of the NRAO.[4] Single-dish continuum and radio recombination line observations (Pauls et al. 1976; Pauls & Mezger 1980; Anantharamaiah & Yusef-Zadeh 1989) have indicated a large number of features having negative radial velocities but distributed at positive longitudes. In particular, the ionized gas is located between the Arc, a prominent radio continuum structure at $l = 0°.2$, and Sgr A West, the ionized gas at $l = 0°.0$, which is believed to be associated with the dynamical center of the Galaxy. Arched filaments of thermal gas at $l = 0°.1$, $b = 0°.08$ (10′ north of Sgr A West) were revealed in VLA images obtained by Yusef-Zadeh, Morris, & Chance (1984). Later, H110α line emission was detected from the arched filaments using the VLA (Yusef-Zadeh 1986; Yusef-Zadeh, Morris, & van Gorkom 1986). A molecular counterpart to the ionized gas has been observed in CS (Serabyn & Güsten 1987), ^{13}CO (Bally et al. 1986), and [C II] (Genzel et al. 1990) in the velocity range -50 to 0 km s^{-1} (hereafter referred to as the -30 km s^{-1} molecular cloud). Neutral hydrogen (H I) absorption observations of the arched filaments show a close association between the continuum and molecular and atomic gas (Lasenby, Lasenby, & Yusef-Zadeh, 1989). The inferred total mass of the entire molecular cloud is $\sim 6 \times 10^5$ $M_\odot$. The ionizing mechanism for this gas has not yet been firmly established.

A number of discrete radio continuum sources (H1–H5 and S1–S2 in Fig. 1) have been identified between the arched filaments and Sgr A West (Yusef-Zadeh & Morris 1987). The H110α line at negative radial velocities has been detected from some of these sources suggesting their association with the -30 km s^{-1} molecular cloud (Yusef-Zadeh 1986). The nature and physical properties of these sources is difficult to determine in the presence of background nonthermal emission. Detailed analysis of these sources would be useful in understanding the ionizing mechanisms in the -30 km s^{-1} molecular cloud.

In this paper we have determined flux densities and infer spectral indices for these discrete radio sources between Sgr A West and the arched filaments based on VLA continuum observations at 20 and 6 cm. Based on H110α and H92α spectral line observations, we present kinematics of ionized gas associated with the discrete sources and argue that these H II regions are related to star formation activity in the -30 km s^{-1} molecular cloud.

2. OBSERVATIONS

The observations reported in this paper provide a useful database for the study of the discrete radio sources H1–H5 (see Fig. 1). Table 1 summarizes parameters of the observations used in this paper. Columns (1) and (2) give the epoch and array configurations of the observations. Columns (3) and (4) give the field centers (B1950). Columns (5) and (6) summarize the wavelengths and bandwidths of the observations, while in column (7) the beam size (FWHM) is listed. For continuum observations, column (8) gives the rms noise in the image. For spectral line observations, columns (8) and (9) give the rms noise in the continuum (see below) and line images, respec-

[1] National Radio Astronomy Observatory, P.O. Box O, Socorro, NM 87131.
[2] Also Department of Physics, University of California, Santa Barbara.
[3] Department of Physics and Astronomy, Northwest University, 2145 North Sheridan Road, Evanston, IL 60208.
[4] The National Radio Astronomy Observatory is operated by Associated Universities, Inc., under cooperative agreement with the National Science Foundation.

TABLE 1

OBSERVATIONAL PARAMETERS

Observation Date (1)	Array (2)	R.A.(1950) (3)	Decl.(1950) (4)	λ_0 (cm) (5)	Bandwidth (MHz) (6)	Beam (FWHM) (7)	rms (c) (mJy beam^{-1}) (8)	rms (l) (mJy beam^{-1}) (9)	Velocity Resolution (km s^{-1}) (10)
1991 Jul 17[a]	A	$17^h42^m30^s.0$	$-28°59'34''$	21/18	3.12	$1'' \times 2''.2$	1	6	10
1989 Oct 24[b]	CnD	17 42 26.0	−28 50 00	3.6	6.25	7	0.3	0.2	7
1988 Jul 8[c]	D	17 42 25.0	−28 57 30	6	12.5	11 × 20	5	0.6	24
1984[d]	BnC	17 43 15.0	−28 52 00	20	12.5	7.5 × 8.7	5	...	...
1986[d]	AnB+BnC+CnD	17 42 35.0	−28 52 40	6	12.5	2.5 × 2.5	0.5	...	...

[a] Observed in a line mode for both H I (1.42 GHz) and OH (1.67 GHz) transitions, centered at $V_{LRS} = 0$ km s^{-1}.
[b] Observed in a line mode for H92α (8.31 GHz), centered at $V_{LRS} = -40$ km s^{-1}.
[c] Observed in a line mode for H110α (4.87 GHz), centered at $V_{LRS} = 0$ km s^{-1}.
[d] Observed in a continuum mode.

tively, and column (10) lists the velocity resolution. All data were reduced using the AIPS softward package. Short remarks on each observations follow the table. We comment in detail on the individual observations below.

2.1. 6 *and* 20 *Centimeter Continuum Observations*

Continuum observations at 20 and 6 cm were carried out in 1984 and 1986 (see Yusef-Zadeh & Morris 1987) using the VLA in several configurations. Three 6 cm continuum observations, performed with the VLA in the hybrid configurations, BnA, CnB, and DnC, were combined to produce a wide field image of size 10′ × 12′; this image was corrected for the effects of primary beam attenuation. A 20 cm continuum image was produced from an observation using the hybrid VLA configuration CnB; at 20 cm, the diffuse extended emission prevalent in the Galactic center region was not resolved resulting in a higher noise level. These images were used to determine flux densities 6 and 20 cm for the sources discussed in this paper.

2.2. 21 *Centimeter Spectral Line Observations*

Spectral line observations at 21 cm were performed in 1991 (Zhao et al. 1992) using the VLA in the A-configuration. Spectral line cubes were produced from each observation. Continuum images were also produced using the central 75% of the observing band for each observation excluding those channels where continuum emission is strongly absorbed. High-resolution images are less sensitive to extended emission which allows more precise flux density determinations for the discrete compact sources.

2.3. H92α *and* H110α *Recombination Line Observations*

Spectral line observations of the H92α and H110α recombination lines were carried out in 1989 and 1988. The VLA was in the DnC configuration for the H92α observations and in the D configuration for the H110α observations.

The flux density calibrator was 3C 286. Amplitude and phase calibration was performed based on the strong point source NRAO 530. NRAO 530 and 3C 286 were used for complex bandpass calibration. Continuum emission subtraction was performed by fitting and removing a continuum background spectrum from each baseline in the visibility domain (see Cornwell et al. 1992). The calibrated visibilities were used to make an image for each spectral channel. Each channel image which contains line emission was cleaned using the Clark-Högbom CLEAN algorithm. The typical rms noise of the cleaned channel image, as stated in Table 1, is 0.2 and 0.6 mJy beam^{-1} at 3.6 and 6 cm, respectively.

3. RESULTS

Continuum images of the H1–H5 sources are shown in Figures 1–4 while Figures 5–9 show neutral hydrogen and RRL spectra of the H1–H5 and S1–S2 sources. The components S1–S2 were detected in H110α emission at velocities of −17 km s^{-1} and −55 km s^{-1} (see Fig. 7), respectively, which are quite distinct from the positive velocity (+70 km s^{-1}) of the streamers. The continuum emission of these components is severely confused by the extended emission from the streamers (see Fig. 1), and therefore the flux densities of these sources were not determined.

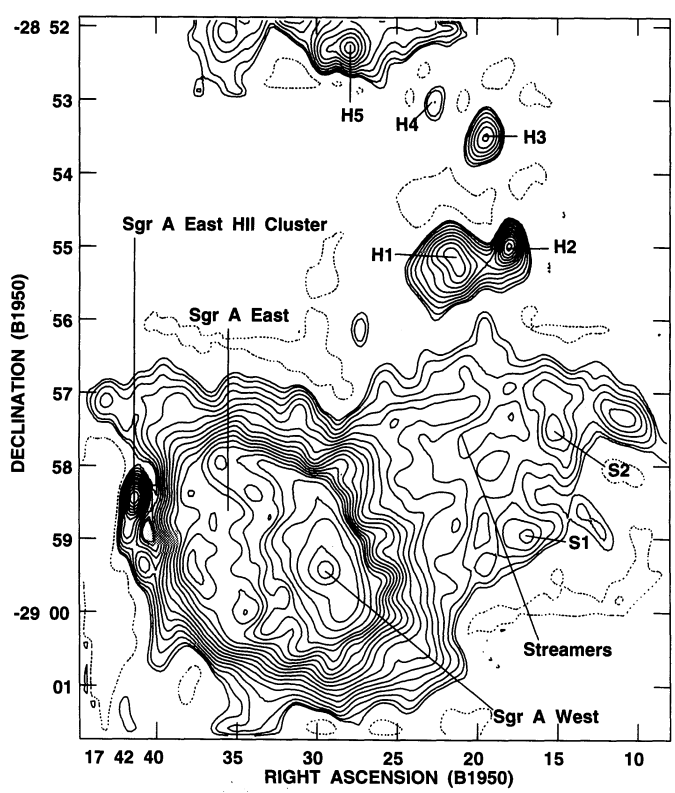

FIG. 1.—Contour plot of 6 cm continuum emission at the Galactic center made from the H110α VLA observations in the D configuration. The beam size (FWHM) is 11″ × 20″ (P.A. = −7°.6). The contours are −0.03, 0.005, 0.01, 0.035, 0.055, 0.08, 0.11, 0.15, 0.19, 0.23, 0.28, 0.34, 0.40, 0.46, 0.53, 0.61, 0.76, 1.1, 1.6, 2.9, and 4.1 Jy beam^{-1}.

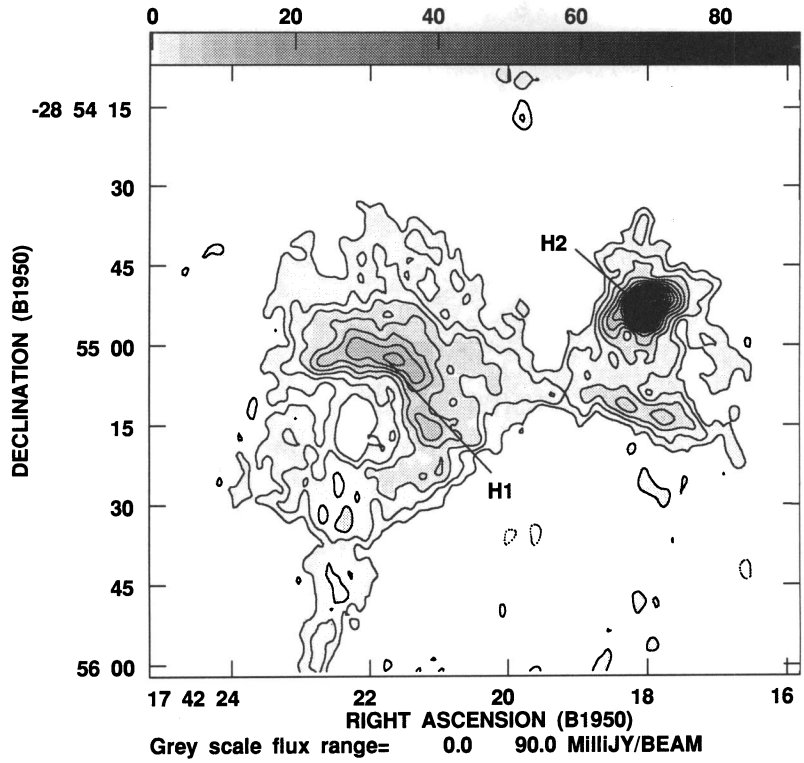

FIG. 2.—Contour plot superposed upon a gray-scale image of 6 cm continuum emission of the sources H1 and H2. This image was made by combining observations using the VLA in its three hybrid configurations: AnB, BnC, and CnD. The beam is circular with a size (FWHM) of 2″.5. The gray scale represents the intensity on a linear scale from 0 to 90 mJy beam^{-1}. The contours are -3, 1, 2, 3.5, 5.5, 8.0, 11, 15, 19, 23, 28, 34, 40, 46, 53, 61, and 69 mJy beam^{-1}.

3.1. *Continuum Images*

In Figure 1, the relative locations (with respect to Sgr A East) of the discrete sources H1–H5, the streamers, and the knots S1 and S2 are shown. The arched filaments are 2′ above the northern boundary of this image. Figures 2 and 4 are 6 cm continuum high-resolution images of the discrete sources H1–H5. Figure 3 is an 18 cm continuum high-resolution image of H2.

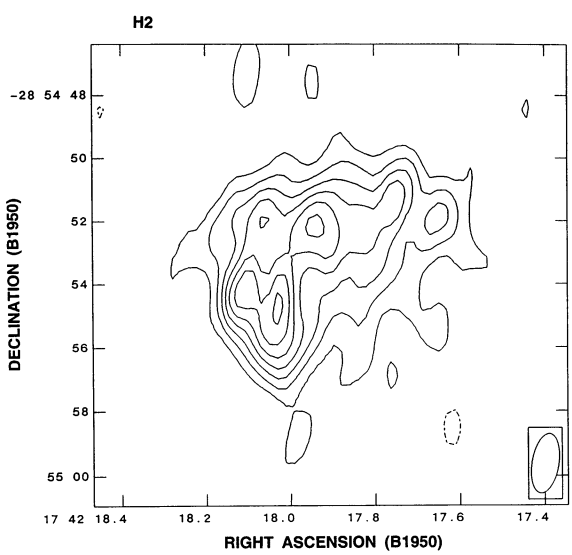

FIG. 3.—Contour plot of 18 cm continuum emission of the source H2. This image was made from OH observations using the VLA in the A-configuration. The beam size (FWHM) is 2″ × 1″ (P.A. = $-10°$) indicated in the lower right-hand corner. The contours are -2.7, 2.7, 4.5, 6.3, 9.9, 12, and 14 mJy beam^{-1}.

3.2. *Spectral Line Images*

In Figure 5 the neutral hydrogen absorption spectra of H2 and Sgr A* are shown. Figure 6 shows the H110α channel images of H1 and H2 over the velocity range -20 to -60 km s^{-1}. Figure 7 shows the spatially integrated H110α emission spectrum for each source. In sources H1–H3 and H5, strong H110α emission was detected. Because of primary beam attenuation, the H110α line was not detected toward H4. The H92α line was detected from sources H3–H5. Figure 8 shows the H92α spectra of H3, H4, H5(E), and H5(W). Figure 9 shows contours of line and continuum intensity, velocity, and LTE electron temperature of H5(E) and H5(W) based upon the H92α observations.

3.3. *Physical Properties*

Table 2 summarizes the continuum properties of the sources H1–H5 determined from the $\lambda = 20$ and 6 cm observations. Columns (1)–(3) identify the coordinates (B1950). Columns (4)–(6) list measured continuum flux densities and a derived $\lambda = 6/20$ cm spectral index ($S \propto \nu^{\alpha}$). In column (7) the angular dimensions are listed. Determination of the flux density was complicated by the presence of background emission. Several methods for determining the flux density were explored. The flux densities of the sources given in Table 2 were determined after correcting for emission arising from the confusing background. Tables 3 and 4 summarize the radio recombination line properties of sources from which line emission was detected. The LTE electron temperatures were derived using formula given by Roelfsma & Goss (1992). Table 5 presents the

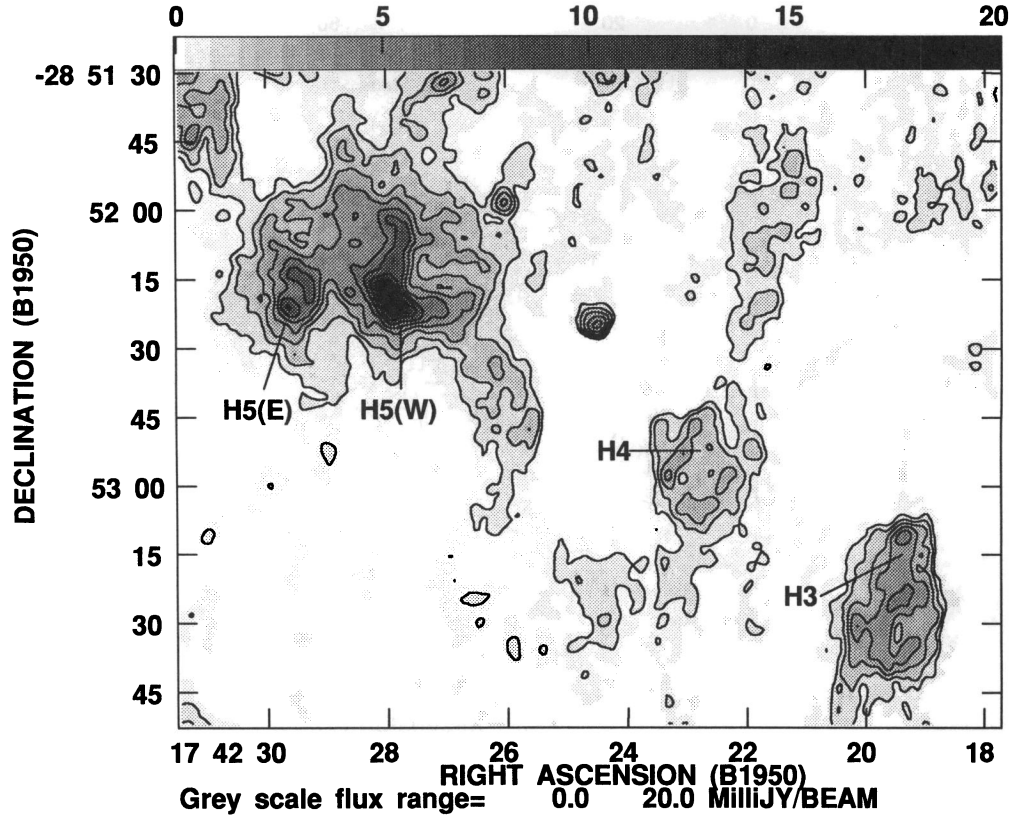

FIG. 4.—Contour plot superposed upon a gray-scale image of 6 cm continuum emission of the sources H3–H5. This image was made by combining observations using the VLA in its three hybrid configurations: AnB, BnC, and CnD. The beam is circular with a size (FWHM) of 2″.5. The gray scale represents the intensity on a linear scale from 0 to 90 mJy beam^{-1}. The contours are -2.4, 0.8, 1.6, 2.8, 4.4, 6.4, 8.8, 12, 15, and 18 mJy beam^{-1}.

derived physical properties of these H II regions. Columns (2) and (3) list the electron density and emission measure derived from H110α observations, while columns (4) and (5) list the excitation parameter and Lyman-continuum photon flux. Spectral types of a single zero-age main-sequence (ZAMS) star are also given in column (6) (Panagia 1973).

4. NOTES ON INDIVIDUAL SOURCES

4.1. *H1*

This source is located just NW of the streamers and has a shell morphology. A central cavity filled with ionized gas is surrounded by an almost complete ring of nonuniform surface brightness. The 6/20 cm spectral index is essentially flat, $\alpha = -0.1$, and H110α emission is detected at a level of 20 σ. The morphology, spectral index, and detection of H110α confirm that this source is an H II region. The physical parameters of this H II region were calculated using the H110α observations. The observed line-to-continuum ratio is 5% indicating an LTE electron temperature T_e^* of 3500 K. Other physical parameters are summarized in Table 5.

The radial velocity of the H110α line emission ($v = -39$ km s^{-1}) matches that of the -30 km s^{-1} molecular cloud which has been observed in CS (Serabyn & Güsten 1987). Since nega-

TABLE 2

PROPERTIES OF CONTINUUM EMISSION

Source (1)	R.A.(1950) (2)	Decl.(1950) (3)	$S_{20\,\mathrm{cm}}$ (mJy) (4)	$S_{6\,\mathrm{cm}}$ (mJy) (5)	α ($S_\nu \propto \nu^\alpha$) (6)	$\theta_{\mathrm{maj}} \times \theta_{\mathrm{min}}$ (7)
H1	17^{h}42^{m}21^s.66	−28°55′02″.4	980 ± 10	880 ± 70	−0.1 ± 0.05	46″ × 16″ [a]
H2	17 42 18.10	−28 54 54.0	280 ± 8$_{18\,\mathrm{cm}}$ [b] 220 ± 10$_{21\,\mathrm{cm}}$ [b]	450 ± 24	0.5 ± 0.05	8 × 5
H3	17 42 19.35	−28 53 11.1	480 ± 11	400 ± 48	−0.15 ± 0.1	30 × 16
H4	17 42 23.31	−28 52 57.6	220 ± 18	210 ± 10	−0.06 ± 0.07	25 × 19
H5(W)	17 42 27.98	−28 52 17.9	1100 ± 60[c]	770 ± 70	−0.01 ± 0.1[d]	35 × 25
H5(E)	17 42 29.65	−28 52 21.1		330 ± 60		30 × 20
S1	17 42 16.77	−28 58 60.0	...	...	...	...
S2	17 42 15.40	−28 57 30.0	...	...	...	...

[a] Shell morphology: inner diameter 16″, outer diameter 46″.
[b] The values are obtained from the VLA high-resolution observations (FWHM ~ 2″ × 1″) at 21 and 18 cm.
[c] The total flux density of H5(W) + H5(E).
[d] The average value of α in the entire H5 region.

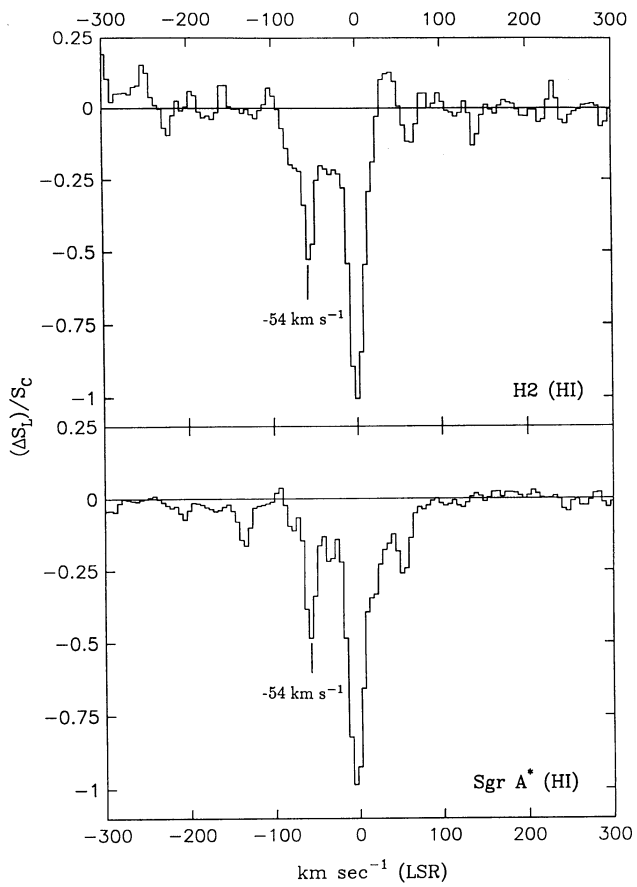

FIG. 5.—Neutral hydrogen absorption spectra from H2 (*upper*) and Sgr A* (*lower*). The line flux density (S_L) has been normalized by the continuum flux density (S_C).

tive velocities are forbidden in the sense of Galactic rotation at this Galactic longitude, the coincident negative velocities in both ionized and molecular gas suggest that H1 is associated with the -30 km s^{-1} molecular cloud.

4.2. *H2*

This source is located to the west of H1 (Fig. 2) and has a comet-like morphology with the head pointing toward H1. This source is unresolved in the 6 cm continuum image and partially resolved in the higher resolution 18 cm continuum image. The 6/20 cm spectral index is inverted, $\alpha = 0.5$, and strong H110α emission is detected at a level of 20 σ. Morphology, spectral index, and detection of H110α confirm that this source is also an H II region.

This H II region is optically thick at 20 cm, with an optical depth $\tau \geq 1$. The observed brightness temperature at 20 cm, $T_b = 3900$ K, is a lower limit to the electron temperature. The line-to-continuum ratio of H110α emission is 5.2%, and the derived electron temperature of 4200 K is consistent with the lower limit provided by the continuum observations.

The 21 cm neutral hydrogen absorption spectra and H110α emission spectra can be used to determine the location of H2 relative to other objects in the Galactic center. The neutral hydrogen absorption spectrum of H2 has two prominent absorption features which are also observed in the neutral hydrogen spectra of Sgr A* (see Fig. 5). The feature at 0 km s^{-1} is attributed to the integrated neutral hydrogen absorption along the path length toward the Galactic center while the features at -54 km s^{-1} can be associated with neutral hydrogen gas in the 3 kpc spiral arm (Liszt, Burton, & van der Hulst 1985). The feature at -135 km s^{-1}, shown in the spectra toward Sgr A*, arises from neutral hydrogen at the front side of the expanding molecular ring (Liszt et al. 1985). This component was not detected toward H2, with an upper limit of $\tau_{\rm H\,I} \approx 0.15$ (3 σ) which approximately equals the optical depth of this component gas observed toward Sgr A* (Liszt et al. 1985; also see Fig. 5). The 21 cm neutral hydrogen spectrum in the direction of source H2 also shows an additional broad absorption feature in the velocity range -80 to -20 km s^{-1}. This broad feature probably arises from absorption by neutral hydrogen gas associated with the -30 km s^{-1} molecular cloud (Lasenby et al. 1989). The presence of these absorption features combined with the negative central velocity of the H110α emission indicate that this region is probably embedded within the -30 km s^{-1} molecular cloud.

TABLE 3

PROPERTIES OF H110α LINES

Source (1)	S_p (mJy) (2)	$V_{\rm LSR}$ (km s^{-1}) (3)	ΔV (km s^{-1}) (4)	T_L/T_C (5)	T_e^* (10^3 K) (6)
H1	64 ± 3	-39 ± 6	42 ± 6	$7.3\% \pm 0.4\%$	3.5 ± 0.5
H2	23 ± 1	-58 ± 6	48 ± 7	5.2 ± 0.4	4.2 ± 0.6
H3	17 ± 1	-42 ± 7	38 ± 8	4.4 ± 0.6	5.9 ± 1
H4	<6	...	...	...	...
H5[a]	41 ± 2	-36 ± 7	46 ± 7	3.7 ± 0.8	5.8 ± 1

[a] Both velocity and angular resolution are not sufficient to separate between the eastern and western components.

TABLE 4

PROPERTIES OF H92α LINES

Source (1)	S_p (mJy) (2)	$V_{\rm LSR}$ (km s^{-1}) (3)	ΔV (km s^{-1}) (4)	T_L/T_C (5)	T_e^* (10^3 K) (6)
H1[a]	...	...	...	...	...
H2[a]	...	...	...	...	...
H3	27 ± 1	-39 ± 2	42 ± 3	7.4 ± 0.4	5.8 ± 0.4
H4	11 ± 0.6	-31 ± 3	42 ± 5	5.8 ± 0.4	7.2 ± 0.9
H5(W)	61 ± 3	-37 ± 2	37 ± 2	8.5 ± 0.6	5.6 ± 0.4
H5(E)	33 ± 2	-28 ± 2	21 ± 2	11 ± 0.8	7.2 ± 0.8

[a] Both H1 and H2 are outside the half-power primary beam.

TABLE 5

PHYSICAL QUANTITIES[a]

Source (1)	N_e (10^3 cm^{-3}) (2)	EM (10^6 pc cm^{-6}) (3)	U (pc cm^{-2}) (4)	log $N_{\rm Lyc}$ (photons s^{-1}) (5)	ZAMS (6)
H1	0.47	0.36	50	49.0	O6
H2	3.1	3.6	40	48.6	O7
H3	0.48	0.30	40	48.5	O7.5
H4	0.36	0.17	33	48.2	O8.5
H5(W)	0.42	0.32	50	48.8	O6.5
H5(E)	0.38	0.22	39	48.4	O8

[a] The quantities are derived from the continuum observations at 6 cm using the model of H II regions discussed by Mezger & Henderson 1967 and Viallefond 1991.

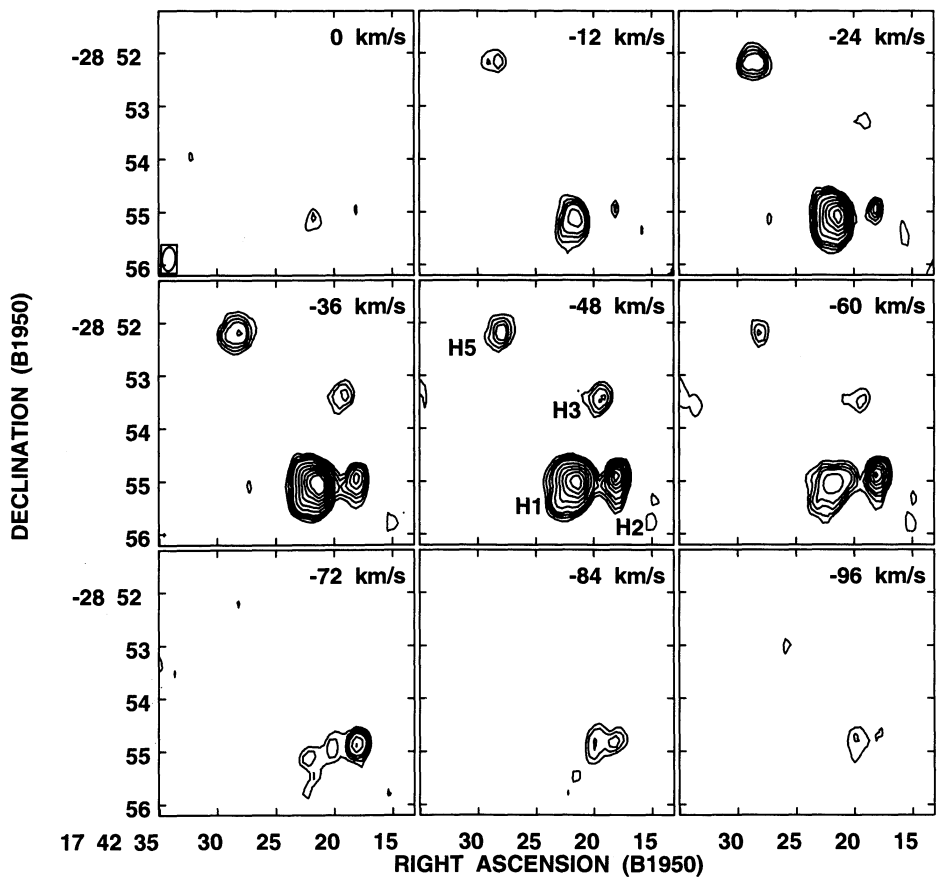

FIG. 6

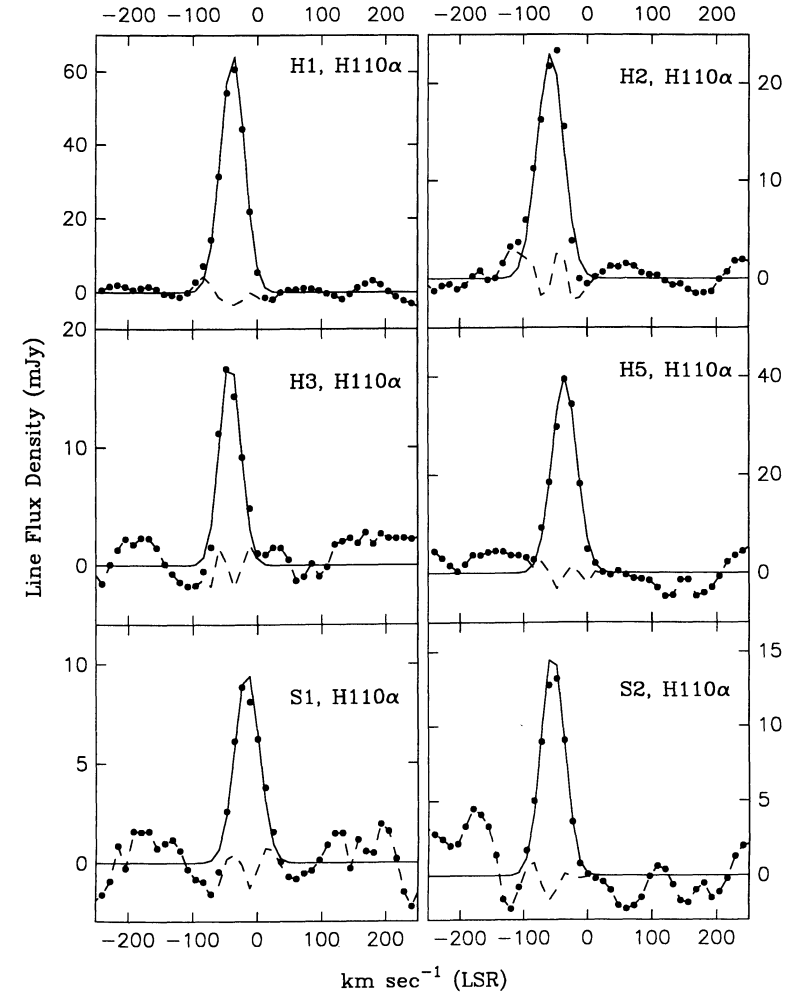

FIG. 7

FIG. 6.—Contour plots of the H110α emission of the sources, H1, H2, H3, and H5, with a channel width of 195 kHz (or 12 km s^{-1}). After Hanning-smoothing, the actual spectral resolution is 24 km^{-1}. This image was made from the H110α observations using the VLA in the D configuration with natural weighting of the visibility data. The beam size (FWHM) is 15″ × 27″ (P.A. = −4°). The rms noise of each channel is ~0.6 mJy beam^{-1} and contours are −2.6, 2.0, 2.6, 3.3, 3.9, 5.2, 7.8, 9.1, 10, and 12 mJy beam^{-1}.

FIG. 7.—Spectral profiles of the H110α line emission of the sources: H1, H2, H3, H5, S1, and S2. After corrections for primary beam attenuation in each spectral channel, the H110α intensities were spatially integrated over the line region of each source to form the profile shown. The profiles were then fitted to Gaussian functions. The solid line represents the fit and the dashed line indicates the residual. The fitted results are summarized in Table 3.

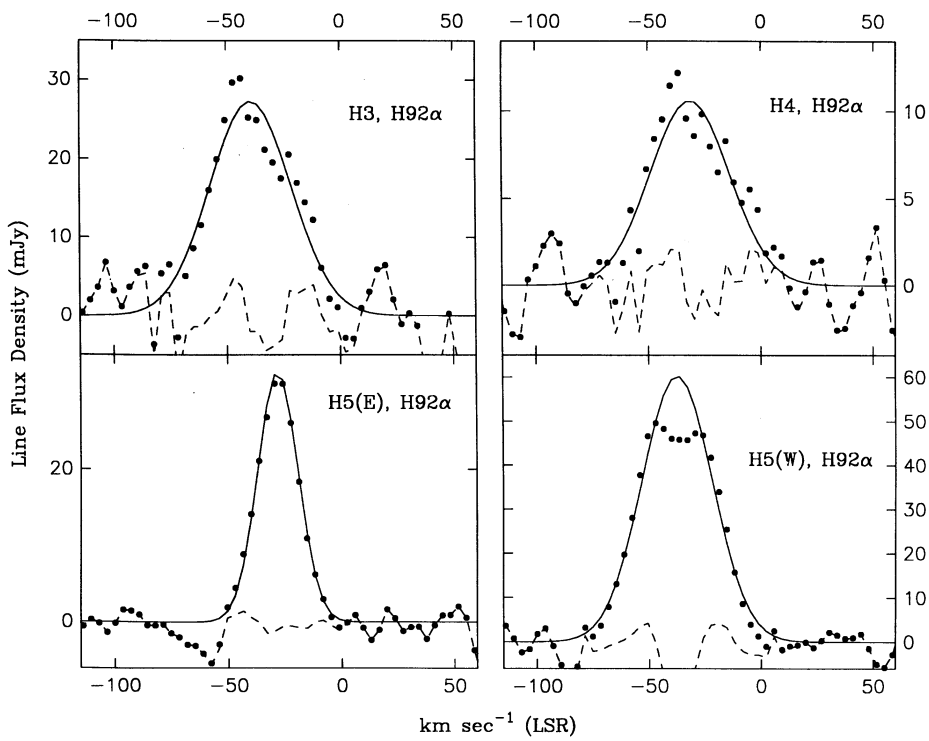

FIG. 8.—Spectral profiles of the H92α line of the sources: H3, H5(E), and H5(W). After corrections from primary beam attenuation in each spectral channel, the H92α intensities were spatially integrated over the line region of each source to form the profile shown. The profiles were then fitted to Gaussian functions. The solid line represents the fit and the dashed line indicates the residual. The fitted results are summarized in Table 4.

4.3. *H3, H4, H5(E), and H5(W)*

The sources H3–H5 are extended with sizes of ~30″ and are located 1′ south of the arched filaments (see Fig. 4). At 6 cm, H3 and H4 are partially resolved and appear slightly elongated in the north-south direction while source H5 consists of two components, H5(E) and H5(W), separated by ~30″. As shown in Figure 4, the two components of H5 appear to have a core-halo morphology.

H5(E) has an extended halo of emission with a core which appears to be an incomplete shell. H5(W) has an extended halo of emission and a core consisting of a peak to the southeast with ridges extending to the north, west, and northeast. The core of H5(W) peaks at the southeastern boundary of the halo emission.

The spectral indices of H3, H4, and H5 are flat ($\alpha \sim 0$) between 6 and 20 cm. H92α and H110α lines were detected from H3 and H5, while the H92α line was detected toward H4. The morphologies and spectra of the sources H3, H4, and H5 combined with the detection of recombination lines confirms that these sources are H II regions.

For H3 and H5, the observed H110α line-to-continuum ratio is ~4%, while the observed H92α line-to-continuum ratio is ~10%. For H4, the H110α was not detected, and the observed H92α line-to-continuum ratio is ~6%. For H5, the LTE electron temperature derived from H92α observations averaged over the source is $T_e^* \sim 5600$ K, in agreement with the value determined from H110α observations.

H3, H4, and H5(W) have broad spectral profiles with a typical width of ~40–50 km s^{-1}, while H5(E) has a width of only ~20 km s^{-1}. These wide spectra are probably due to velocity gradients across the source; such a gradient is observed in H5(W) in a SE-NW direction (see Fig. 9). The velocity ranges from −50 km s^{-1} at the NW boundary to −30 m s^{-1} at the SE edge. The negative central velocity indicates that these sources are probably associated with the −30 km s^{-1} molecular cloud.

5. DISCUSSION

The detection of hydrogen recombination line emission toward H1–H5 indicates that these sources are H II regions. There are not yet any detections of helium recombination lines toward these sources. Assuming an abundance of singly ionized helium $Y^+ \sim 0.1$, LTE electron temperatures of $T_e^* \sim$ 3500–7200 K are estimated (following Roelfesma & Goss 1992); an absence of singly ionized helium would indicate that the inferred temperature, T_e^*, was underestimated by ~10%. The low temperatures, 3500–6000 K, are atypical when compared with other H II regions in the Galactic disk. However, similar LTE T_e^*'s of 3500–6600 K have also been determined toward some H II regions in Sgr B1 (at $l = 0\overset{\circ}{.}5$, $b = 0\overset{\circ}{.}0$), a star-forming region near the Galactic center (Mehringer et al. 1992). The inferred low electron temperatures probably indicate relatively high metal abundances in these H II regions (e.g., Shaver, McGee, & Pottasch 1979). Using the H110α recombination line and continuum observations at 6 cm, the inferred physical parameters of these H II regions given in Table 5 have been derived (Mezger & Henderson 1967; Vaillefond 1991).

The dominant ionization mechanism for these H II regions is photoionization. Observationally, there is no indication of strong interactions between these discrete H II regions and magnetic fields; therefore, magnetohydrodynamic processes are unlikely to be the major source of ionization. Radio recombination line could be produced by fast J-type shocks in molecular clouds (e.g., McKee & Hollenbach 1987). The flux of

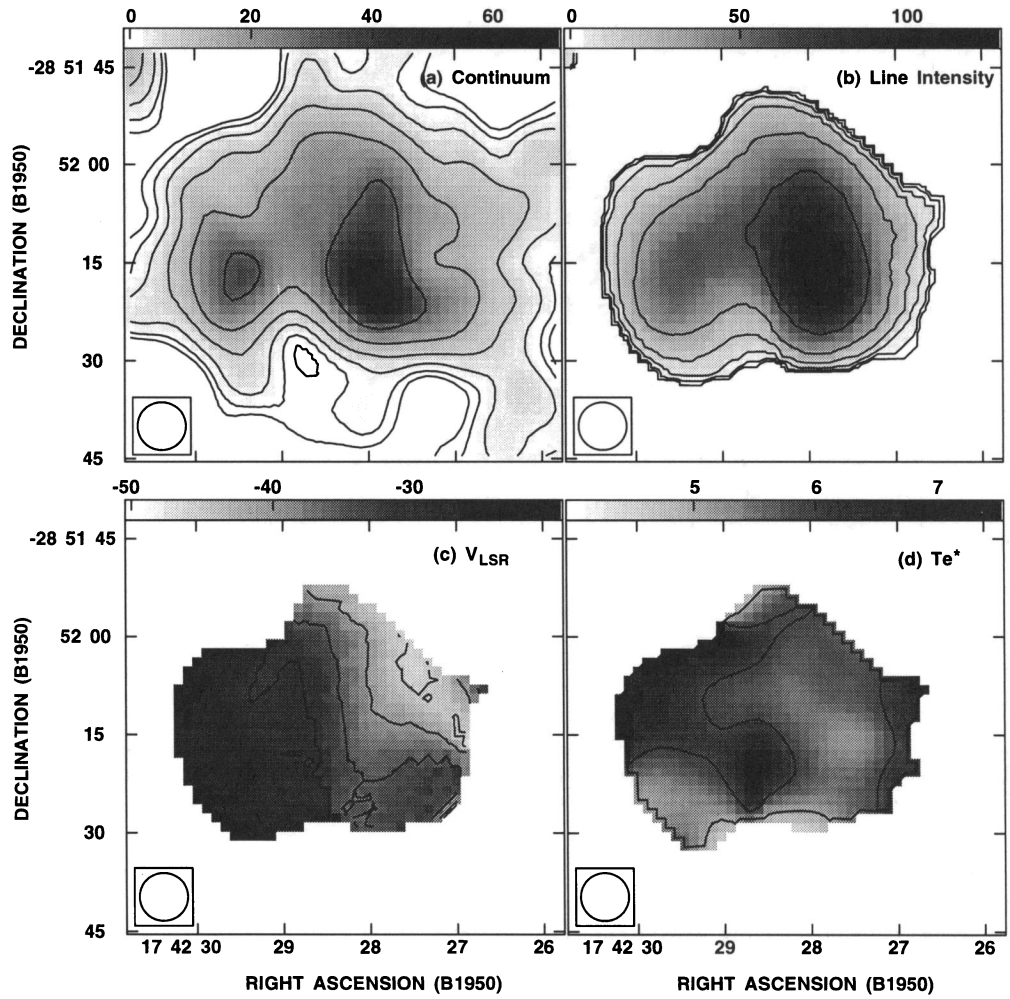

FIG. 9.—Contour plots and gray-scale image of the source H5, made from the VLA H92α observations. The beam size (FWHM) is ~7″, indicated in the bottom left-hand corners. (*a*) 3.6 cm continuum emission with a linear gray scale from 0 to 70 mJy beam^{-1} and contours are 1, 2, 4, 8, 16, 32, and 64 mJy beam^{-1}. (*b*) The spatial distribution of the velocity-integrated H92α line; the gray scale is linear in intensity from 0 to 120 Jy beam^{-1} m s^{-1} and contours are 2, 4, 8, 16, 32, 64, 96, and 130 Jy beam^{-1} m s^{-1}. (*c*) The spatial distribution of velocity obtained from a moment analysis; the gray scale is linear in velocity from −50 to −20 km s^{-1} and contours are −25, −30, −35, −40, and −45 km s^{-1}. (*d*) The spatial distribution of the LTE electron temperature (T_e^*); the gray scale is linear in T_e^* from 4000 to 7500 K and contours are 5000, 6000, and 7000 K.

ionizing photons produced by shocks in the stellar wind are, however, a few orders of magnitude less than the UV photon flux (10^{48-49} photons s^{-1}) generated by an OB main-sequence star; the shocks are far less effective at producing recombination lines than are massive stars (McKee & Hollenbach 1987). Although the morphologies of these H II regions do show indications of shock fronts, the observed radio recombination line flux densities at 3.5 and 6 cm are too strong to be produced through the shock processes. Shock ionization can be ruled out as the principal mechanism of ionization.

The morphologies of H1–H5 are similar to those of H II regions seen in other star formation regions, such as Sgr B1 near the Galactic center (Mehringer et al. 1992). The incomplete shell-type morphology of the source H1 can be explained by a champagne-type outflow (Tenorio-Tagle, Yorke, & Bodenheimer 1979). Such an outflow would be expected if the ionization front of the embedded H II region expands beyond the edge of its parent molecular cloud. The large radial velocity width of H110α emission (40 km s^{-1}) for source H1 is probably due to a velocity gradient; this is consistent with that expected in a champagne expansion. The champagne expansion phase of an OB star and molecular cloud association is expected from theoretical models to be a long-lived phenomena. Cometary morphology similar to that observed in H2 occurs in ~20% of ultracompact H II regions (Wood & Churchwell 1989) and is thought to result from the supersonic motion of a hot star and its surrounding H II region through a cooler ambient medium. Numerical simulations show that a bow shock forms in front of the moving star and appears as the head of a cometary structure (Mac Low et al. 1991).

The negative radial velocities observed in the radio recombination lines from H1–H5 are evidence for association with the −30 km s^{-1} molecular cloud. The molecular cloud lies to the north of Sgr A West and has been imaged in CS at −80 to 0 km s^{-1} (Serabyn & Güsten 1987).

Comparison of [C II] emission, dust emission, and the ionized gas distribution indicates that the gas and dust are spatially correlated. Comparison of the spatial distribution of [C II] 158 μm (Genzel et al. 1990) and the thermal radio continuum show that H1 and H2 correspond to a [C II] peak at G−0.01+0.02 while H5 is close to a [C II] peak at G0.07+0.04. A local increase of far-infrared emission at

G−0.01+0.02 and G0.07+0.04 have been observed by Gatley et al. (1977, 1978) at 30, 50, and 100 μm and by Dent et al. (1982) at 55 and 125 μm with higher sensitivities than those in the earlier observations. The derived dust temperature distribution based on 55/125 μm observations shows a 70 K peak at Sgr A West with subsidiary 50 K peaks near H1, H2, and H5, while the rest of the molecular cloud region is below 40 K. As pointed out by Cox & Mezger (1991), the colder dust is clearly correlated with the molecular gas while the warmer dust is associated with the ionized gas.

In addition, the infrared excess (IRE), defined as the ratio of infrared luminosity to Lyman-continuum flux, is a measure of the heating of dust associated with H II regions. Based on a far-infrared survey of the Galactic center at 1′ resolution at 40–250 μm and radio observations at 15 GHz with a similar angular resolution, Odenwald & Fazio (1984) found that the IREs of G−0.01+0.02 and G0.07+0.04 are 15 and 6, respectively. The values are in agreement with those obtained from earlier FIR observations (Gatley et al. 1978) but are considerably less than the IRE of 30 determined for the diffuse FIR component, within the inner 400 pc of the Galaxy, which is presumably heated by a population of K and M giants (Cox & Laureijs 1989). The IREs of G−0.01+0.02 and G0.07+0.04 are comparable to the values found for the Galactic plane H II regions (Myers et al. 1986), suggesting that the enhanced far-infrared radiation from the two regions could be powered by small numbers of early-type O stars. The far-infrared results appear to be consistent with the hypothesis that the H II regions H1–H5 are the sites of recent formation of early-type stars.

6. CONCLUSIONS

On the basis of recombination line observations, morphology, and inferred LTE electron temperatures, the sources H1–H5 are confirmed to be H II regions. Radial velocities of their recombination lines indicate that they are located within the -30 km s^{-1} molecular cloud. The electron densities and temperatures of these regions imply that the principal ionizing mechanism is photoionization, probably by OB type stars recently formed within the molecular cloud. It is clear that the negative radial velocity molecular cloud is one of the most productive sites of star formation near the Galactic center. The kinematics of the arched filaments are complex and will be discussed in Paper II in this series (Zhao et al. 1993).

We would like to gratefully acknowledge P. Palmer and D. Mehringer for helpful discussions and comments.

REFERENCES

Anantharamaiah, K. R., & Yuseh-Zadeh, F. 1989, in IAU Symp. 136, The Center of The Galaxy, ed. M. Morris (Dordrecht: Kluwer), 159
Armstrong, J. T., Jackson, J. M., & Ho, P. T. P. 1989, in IAU Symp. 136, The Center of The Galaxy, ed. M. Morris (Dordrecht: Kluwer), 389
Bally, J., Stark, A. A., Wilson, R. W., & Henkel, C. 1987, ApJS, 65, 13
Cornwell, T. J., Uson, J. M., & Haddad, N. 1992, A&A, 258, 583
Cox, P., & Laureijs, R. 1989, in IAU Symp. 136, The Center of The Galaxy, ed. M. Morris (Dordrecht: Kluwer), 121
Cox, P., & Mezger, P. G. 1989, Astron. Astrophys. Rev., 1, 49
Dent, W. A., Werner, M. W., Gatley, I., Becklin, E. E., Hildebrand, R. H., Keene, J., & Whitcomb, S. E. 1982, in The Galactic Center, ed. G. R. Riegler & R. D. Blandford (A.I.P. Conf. Proc. 83) (New York: AIP), 33
Ekers, R. D., van Gorkom, J. H., Schwarz, U. J., & Goss, W. M. 1983, A&A, 122, 143
Gatley, I., Becklin, E. E., Werner, M. W., & Harper, D. A. 1978, ApJ, 220, 822
Gatley, I., Becklin, E. E., Werner, M. W., & Wynn-Williams, C. G. 1977, ApJ, 216, 277
Genzel, R., Stacey, G. J., Harris, A. I., Townes, C. H., Geis, N., Graff, U. U., Poglitsch, A., & Stutzki, J. 1990, ApJ, 356, 160
Goss, W. M., Schwarz, U. J., van Gorkom, J. H., & Ekers, R. D. 1985, MNRAS, 215, 69P
Ho, P. T. P., Jackson, J. M., Barrett, A. H., & Armstrong, J. T. 1985, ApJ, 288, 575
Lasenby, J., Lasenby, A. N., & Yusef-Zadeh, F. 1989, ApJ, 343, 177
Liszt, H. S., Burton, W. B., & van der Hulst, J. M. 1985, A&A, 142, 245
Mac Low, M.-M., Van Buren, D., Wood, D. O. S., & Churchwell, E. 1991, ApJ, 369, 395
McKee, C. F., & Hollenbach, D. J. 1987, 322, 275
Mehriger, D., Yusef-Zadeh, F., Palmer, P., & Goss, W. M. 1992, ApJ, 401, 168
Mezger, P., & Henderson, A. 1967, ApJ, 147, 471
Myers, P. C., Dame, T. M., Thaddeus, P., Cohen, R. S., Silverberg, R. F., Dwek, E., & Hauser, M. G. 1986, ApJ, 301, 398
Odenwald, S. F., & Fazio, G. G. 1984, ApJ, 283, 601
Pauls, T., Downes, D., Mezger, P. G., & Churchwell, E. 1976, A&A, 46, 407
Pauls, T., & Mezger, P. G. 1980, A&A, 85, 26
Panagia, N. 1973, ApJ, 78, 929
Roelfsema, P. R., & Goss, W. M. 1992, Astron. Astrophys. Rev., 4, 161
Serabyn, E., & Güsten, R. 1987, A&A, 184, 133
Shaver, P. A., McGee, R. X., & Pottasch, S. R. 1979, Nature, 280, 476
Tenorio-Tagle, G., Yorke, H. W., & Bodenheimer, P. 1979, A&A, 80, 110
Viallefond, F. 1991, private communication
Wood, D. O. S., & Churchwell, E. 1989, ApJS, 69, 831
Yusef-Zadeh, F. 1986, Ph.D. thesis, Columbia Univ.
Yusef-Zadeh, F., & Morris, M. 1987, ApJ, 320, 545
Yusef-Zadeh, F., Morris, M., & Chance, D. 1984, Nature, 310, 557
Yusef-Zadeh, F., Morris, M., & van Gorkom, J. H. 1986, in The Galactic Center, ed. D. C. Backer (A.I.P. Conf. Proc. 155) (New York: AIP), 190
Zhao, J.-H., et al. 1992, Science, 255, 1481
Zhao, J.-H., et al. 1993, in preparation (Paper II)